Large scale distribution of ultra high energy cosmic rays detected at the Pierre Auger Observatory with zenith angles up to 80°

The Pierre Auger Collaboration

A. Aab[42], P. Abreu[64], M. Aglietta[53], E.J. Ahn[81], I. Al Samarai[29], I.F.M. Albuquerque[17], I. Allekotte[1], J. Allen[84], P. Allison[86], A. Almela[11, 8], J. Alvarez Castillo[57], J. Alvarez-Muñiz[74], R. Alves Batista[41], M. Ambrosio[44], A. Aminaei[58], L. Anchordoqui[80], S. Andringa[64], C. Aramo[44], V.M. Aranda[71], F. Arqueros[71], H. Asorey[1], P. Assis[64], J. Aublin[31], M. Ave[1], M. Avenier[32], G. Avila[10], N. Awal[84], A.M. Badescu[68], K.B. Barber[12], J. Bäuml[36], C. Baus[36], J.J. Beatty[86], K.H. Becker[35], J.A. Bellido[12], C. Berat[32], M.E. Bertaina[53], X. Bertou[1], P.L. Biermann[39], P. Billoir[31], S.G. Blaess[12], M. Blanco[31], C. Bleve[48], H. Blümer[36, 37], M. Boháčová[27], D. Boncioli[52], C. Bonifazi[23], R. Bonino[53], N. Borodai[62], J. Brack[78], I. Brancus[65], A. Bridgeman[37], P. Brogueira[64], W.C. Brown[79], P. Buchholz[42], A. Bueno[73], S. Buitink[58], M. Buscemi[44], K.S. Caballero-Mora[55 e], B. Caccianiga[43], L. Caccianiga[31], M. Candusso[45], L. Caramete[39], R. Caruso[46], A. Castellina[53], G. Cataldi[48], L. Cazon[64], R. Cester[47], A.G. Chavez[56], A. Chiavassa[53], J.A. Chinellato[18], J. Chudoba[27], M. Cilmo[44], R.W. Clay[12], G. Cocciolo[48], R. Colalillo[44], A. Coleman[87], L. Collica[43], M.R. Coluccia[48], R. Conceição[64], F. Contreras[9], M.J. Cooper[12], A. Cordier[30], S. Coutu[87], C.E. Covault[76], J. Cronin[88], A. Curutiu[39], R. Dallier[34, 33], B. Daniel[18], S. Dasso[5, 3], K. Daumiller[37], B.R. Dawson[12], R.M. de Almeida[24], M. De Domenico[46], S.J. de Jong[58, 60], J.R.T. de Mello Neto[23], I. De Mitri[48], J. de Oliveira[24], V. de Souza[16], L. del Peral[72], O. Deligny[29], H. Dembinski[37], N. Dhital[83], C. Di Giulio[45], A. Di Matteo[49], J.C. Diaz[83], M.L. Díaz Castro[18], F. Diogo[64], C. Dobrigkeit[18], W. Docters[59], J.C. D'Olivo[57], A. Dorofeev[78], Q. Dorosti Hasankiadeh[37], M.T. Dova[4], J. Ebr[27], R. Engel[37], M. Erdmann[40], M. Erfani[42], C.O. Escobar[81, 18], J. Espadanal[64], A. Etchegoyen[8, 11], P. Facal San Luis[88], H. Falcke[58, 61, 60], K. Fang[88], G. Farrar[84], A.C. Fauth[18], N. Fazzini[81], A.P. Ferguson[76], M. Fernandes[23], B. Fick[83], J.M. Figueira[8], A. Filevich[8], A. Filipčič[69, 70], B.D. Fox[89], O. Fratu[68], M.M. Freire[6], U. Fröhlich[42], B. Fuchs[36], T. Fujii[88], R. Gaior[31], B. García[7], D. Garcia-Gamez[30], D. Garcia-Pinto[71], G. Garilli[46], A. Gascon Bravo[73], F. Gate[34], H. Gemmeke[38], P.L. Ghia[31], U. Giaccari[23], M. Giammarchi[43], M. Giller[63], C. Glaser[40], H. Glass[81], M. Gómez Berisso[1], P.F. Gómez Vitale[10], P. Gonçalves[64], J.G. Gonzalez[36], N. González[8], B. Gookin[78], J. Gordon[86], A. Gorgi[53], P. Gorham[89], P. Gouffon[17], S. Grebe[58, 60], N. Griffith[86], A.F. Grillo[52], T.D. Grubb[12], F. Guarino[44], G.P. Guedes[19], M.R. Hampel[8], P. Hansen[4], D. Harari[1], T.A. Harrison[12], S. Hartmann[40], J.L. Harton[78], A. Haungs[37], T. Hebbeker[40], D. Heck[37], P. Heimann[42], A.E. Herve[37], G.C. Hill[12], C. Hojvat[81], N. Hollon[88], E. Holt[37], P. Homola[35], J.R. Hörandel[58, 60], P. Horvath[28], M. Hrabovský[28, 27], D. Huber[36], T. Huege[37], A. Insolia[46], P.G. Isar[66], I. Jandt[35], S. Jansen[58, 60], C. Jarne[4], M. Josebachuili[8], A. Kääpä[35], O. Kambeitz[36], K.H. Kampert[35], P. Kasper[81], I. Katkov[36], B. Kégl[30], B. Keilhauer[37], A. Keivani[87], E. Kemp[18], R.M. Kieckhafer[83], H.O. Klages[37], M. Kleifges[38], J. Kleinfeller[9], R. Krause[40], N. Krohm[35], O. Krömer[38], D. Kruppke-Hansen[35], D. Kuempel[40], N. Kunka[38], D. LaHurd[76], L. Latronico[53], R. Lauer[91], M. Lauscher[40], P. Lautridou[34], S. Le Coz[32], M.S.A.B. Leão[14], D. Lebrun[32], P. Lebrun[81], M.A. Leigui de Oliveira[22], A. Letessier-Selvon[31], I. Lhenry-Yvon[29], K. Link[36], R. López[54],

K. Louedec[32], J. Lozano Bahilo[73], L. Lu[35, 75], A. Lucero[8], M. Ludwig[36], M. Malacari[12], S. Maldera[53], M. Mallamaci[43], J. Maller[34], D. Mandat[27], P. Mantsch[81], A.G. Mariazzi[4], V. Marin[34], I.C. Mariş[73], G. Marsella[48], D. Martello[48], L. Martin[34, 33], H. Martinez[55], O. Martínez Bravo[54], D. Martraire[29], J.J. Masías Meza[3], H.J. Mathes[37], S. Mathys[35], J. Matthews[82], J.A.J. Matthews[91], G. Matthiae[45], D. Maurel[36], D. Maurizio[13], E. Mayotte[77], P.O. Mazur[81], C. Medina[77], G. Medina-Tanco[57], R. Meissner[40], M. Melissas[36], D. Melo[8], A. Menshikov[38], S. Messina[59], R. Meyhandan[89], S. Mićanović[25], M.I. Micheletti[6], L. Middendorf[40], I.A. Minaya[71], L. Miramonti[43], B. Mitrica[65], L. Molina-Bueno[73], S. Mollerach[1], M. Monasor[88], D. Monnier Ragaigne[30], F. Montanet[32], C. Morello[53], M. Mostafá[87], C.A. Moura[22], M.A. Muller[18, 21], G. Müller[40], S. Müller[37], M. Münchmeyer[31], R. Mussa[47], G. Navarra[53] ‡, S. Navas[73], P. Necesal[27], L. Nellen[57], A. Nelles[58, 60], J. Neuser[35], P.H. Nguyen[12], M. Niechciol[42], L. Niemietz[35], T. Niggemann[40], D. Nitz[83], D. Nosek[26], V. Novotny[26], L. Nožka[28], L. Ochilo[42], F. Oikonomou[87], A. Olinto[88], M. Oliveira[64], N. Pacheco[72], D. Pakk Selmi-Dei[18], M. Palatka[27], J. Pallotta[2], N. Palmieri[36], P. Papenbreer[35], G. Parente[74], A. Parra[54], T. Paul[80, 85], M. Pech[27], J. Pękala[62], R. Pelayo[54] *d*, I.M. Pepe[20], L. Perrone[48], E. Petermann[90], C. Peters[40], S. Petrera[49, 50], Y. Petrov[78], J. Phuntsok[87], R. Piegaia[3], T. Pierog[37], P. Pieroni[3], M. Pimenta[64], V. Pirronello[46], M. Platino[8], M. Plum[40], A. Porcelli[37], C. Porowski[62], R.R. Prado[16], P. Privitera[88], M. Prouza[27], V. Purrello[1], E.J. Quel[2], S. Querchfeld[35], S. Quinn[76], J. Rautenberg[35], O. Ravel[34], D. Ravignani[8], B. Revenu[34], J. Ridky[27], S. Riggi[46], M. Risse[42], P. Ristori[2], V. Rizi[49], W. Rodrigues de Carvalho[74], G. Rodriguez Fernandez[45], J. Rodriguez Rojo[9], M.D. Rodríguez-Frías[72], D. Rogozin[37], G. Ros[72], J. Rosado[71], T. Rossler[28], M. Roth[37], E. Roulet[1], A.C. Rovero[5], S.J. Saffi[12], A. Saftoiu[65], F. Salamida[29], H. Salazar[54], A. Saleh[70], F. Salesa Greus[87], G. Salina[45], F. Sánchez[8], P. Sanchez-Lucas[73], C.E. Santo[64], E. Santos[18], E.M. Santos[17], F. Sarazin[77], B. Sarkar[35], R. Sarmento[64], R. Sato[9], N. Scharf[40], V. Scherini[48], H. Schieler[37], P. Schiffer[41], D. Schmidt[37], O. Scholten[59] *f*, H. Schoorlemmer[89, 58, 60], P. Schovánek[27], A. Schulz[37], J. Schulz[58], J. Schumacher[40], S.J. Sciutto[4], A. Segreto[51], M. Settimo[31], A. Shadkam[82], R.C. Shellard[13], I. Sidelnik[1], G. Sigl[41], O. Sima[67], A. Śmiałkowski[63], R. Šmída[37], G.R. Snow[90], P. Sommers[87], J. Sorokin[12], R. Squartini[9], Y.N. Srivastava[85], S. Stanič[70], J. Stapleton[86], J. Stasielak[62], M. Stephan[40], A. Stutz[32], F. Suarez[8], T. Suomijärvi[29], A.D. Supanitsky[5], M.S. Sutherland[86], J. Swain[85], Z. Szadkowski[63], M. Szuba[37], O.A. Taborda[1], A. Tapia[8], A. Tepe[42], V.M. Theodoro[18], C. Timmermans[60, 58], C.J. Todero Peixoto[15], G. Toma[65], L. Tomankova[37], B. Tomé[64], A. Tonachini[47], G. Torralba Elipe[74], D. Torres Machado[23], P. Travnicek[27], E. Trovato[46], R. Ulrich[37], M. Unger[37, 84], M. Urban[40], J.F. Valdés Galicia[57], I. Valiño[74], L. Valore[44], G. van Aar[58], P. van Bodegom[12], A.M. van den Berg[59], S. van Velzen[58], A. van Vliet[41], E. Varela[54], B. Vargas Cárdenas[57], G. Varner[89], J.R. Vázquez[71], R.A. Vázquez[74], D. Veberič[30], V. Verzi[45], J. Vicha[27], M. Videla[8], L. Villaseñor[56], B. Vlcek[72], S. Vorobiov[70], H. Wahlberg[4], O. Wainberg[8, 11], D. Walz[40], A.A. Watson[75], M. Weber[38], K. Weidenhaupt[40], A. Weindl[37], F. Werner[36], A. Widom[85], L. Wiencke[77], B. Wilczyńska[62] ‡, H. Wilczyński[62], C. Williams[88], T. Winchen[35], D. Wittkowski[35], B. Wundheiler[8], S. Wykes[58], T. Yamamoto[88] *a*, T. Yapici[83], G. Yuan[82], A. Yushkov[42], B. Zamorano[73], E. Zas[74], D. Zavrtanik[70, 69], M. Zavrtanik[69, 70],

A. Zepeda[55] [b], J. Zhou[88], Y. Zhu[38], M. Zimbres Silva[18], M. Ziolkowski[42], F. Zuccarello[46]

[1] Centro Atómico Bariloche and Instituto Balseiro (CNEA-UNCuyo-CONICET), San Carlos de Bariloche, Argentina

[2] Centro de Investigaciones en Láseres y Aplicaciones, CITEDEF and CONICET, Argentina

[3] Departamento de Física, FCEyN, Universidad de Buenos Aires and CONICET, Argentina

[4] IFLP, Universidad Nacional de La Plata and CONICET, La Plata, Argentina

[5] Instituto de Astronomía y Física del Espacio (IAFE, CONICET-UBA), Buenos Aires, Argentina

[6] Instituto de Física de Rosario (IFIR) - CONICET/U.N.R. and Facultad de Ciencias Bioquímicas y Farmacéuticas U.N.R., Rosario, Argentina

[7] Instituto de Tecnologías en Detección y Astropartículas (CNEA, CONICET, UNSAM), and Universidad Tecnológica Nacional - Facultad Regional Mendoza (CONICET, CNEA), Mendoza, Argentina

[8] Instituto de Tecnologías en Detección y Astropartículas (CNEA, CONICET, UNSAM), Buenos Aires, Argentina

[9] Observatorio Pierre Auger, Malargüe, Argentina

[10] Observatorio Pierre Auger and Comisión Nacional de Energía Atómica, Malargüe, Argentina

[11] Universidad Tecnológica Nacional - Facultad Regional Buenos Aires, Buenos Aires, Argentina

[12] University of Adelaide, Adelaide, S.A., Australia

[13] Centro Brasileiro de Pesquisas Fisicas, Rio de Janeiro, RJ, Brazil

[14] Faculdade Independente do Nordeste, Vitória da Conquista, Brazil

[15] Universidade de São Paulo, Escola de Engenharia de Lorena, Lorena, SP, Brazil

[16] Universidade de São Paulo, Instituto de Física de São Carlos, São Carlos, SP, Brazil

[17] Universidade de São Paulo, Instituto de Física, São Paulo, SP, Brazil

[18] Universidade Estadual de Campinas, IFGW, Campinas, SP, Brazil

[19] Universidade Estadual de Feira de Santana, Brazil

[20] Universidade Federal da Bahia, Salvador, BA, Brazil

[21] Universidade Federal de Pelotas, Pelotas, RS, Brazil

[22] Universidade Federal do ABC, Santo André, SP, Brazil

[23] Universidade Federal do Rio de Janeiro, Instituto de Física, Rio de Janeiro, RJ, Brazil

[24] Universidade Federal Fluminense, EEIMVR, Volta Redonda, RJ, Brazil

[25] Rudjer Bošković Institute, 10000 Zagreb, Croatia

[26] Charles University, Faculty of Mathematics and Physics, Institute of Particle and Nuclear Physics, Prague, Czech Republic

[27] Institute of Physics of the Academy of Sciences of the Czech Republic, Prague, Czech Republic

[28] Palacky University, RCPTM, Olomouc, Czech Republic

[29] Institut de Physique Nucléaire d'Orsay (IPNO), Université Paris 11, CNRS-IN2P3, France

[30] Laboratoire de l'Accélérateur Linéaire (LAL), Université Paris 11, CNRS-IN2P3, France

[31] Laboratoire de Physique Nucléaire et de Hautes Energies (LPNHE), Universités Paris 6 et Paris 7, CNRS-IN2P3, Paris, France

[32] Laboratoire de Physique Subatomique et de Cosmologie (LPSC), Université Grenoble-Alpes, CNRS/IN2P3, France

[33] Station de Radioastronomie de Nançay, Observatoire de Paris, CNRS/INSU, France

[34] SUBATECH, École des Mines de Nantes, CNRS-IN2P3, Université de Nantes, France

[35] Bergische Universität Wuppertal, Wuppertal, Germany

[36] Karlsruhe Institute of Technology - Campus South - Institut für Experimentelle Kernphysik (IEKP), Karlsruhe, Germany

[37] Karlsruhe Institute of Technology - Campus North - Institut für Kernphysik, Karlsruhe, Germany

[38] Karlsruhe Institute of Technology - Campus North - Institut für Prozessdatenverarbeitung und Elektronik, Karlsruhe, Germany

[39] Max-Planck-Institut für Radioastronomie, Bonn, Germany

[40] RWTH Aachen University, III. Physikalisches Institut A, Aachen, Germany

[41] Universität Hamburg, Hamburg, Germany

[42] Universität Siegen, Siegen, Germany

[43] Università di Milano and Sezione INFN, Milan, Italy

[44] Università di Napoli "Federico II" and Sezione INFN, Napoli, Italy

[45] Università di Roma II "Tor Vergata" and Sezione INFN, Roma, Italy

[46] Università di Catania and Sezione INFN, Catania, Italy

[47] Università di Torino and Sezione INFN, Torino, Italy

[48] Dipartimento di Matematica e Fisica "E. De Giorgi" dell'Università del Salento and Sezione INFN, Lecce, Italy

[49] Dipartimento di Scienze Fisiche e Chimiche dell'Università dell'Aquila and INFN, Italy

[50] Gran Sasso Science Institute (INFN), L'Aquila, Italy

[51] Istituto di Astrofisica Spaziale e Fisica Cosmica di Palermo (INAF), Palermo, Italy

[52] INFN, Laboratori Nazionali del Gran Sasso, Assergi (L'Aquila), Italy

[53] Osservatorio Astrofisico di Torino (INAF), Università di Torino and Sezione INFN, Torino, Italy

[54] Benemérita Universidad Autónoma de Puebla, Puebla, México

[55] Centro de Investigación y de Estudios Avanzados del IPN (CINVESTAV), México, México

[56] Universidad Michoacana de San Nicolás de Hidalgo, Morelia, Michoacán, México

[57] Universidad Nacional Autónoma de México, México, D.F., México

[58] IMAPP, Radboud University Nijmegen, Netherlands

[59] KVI - Center for Advanced Radiation Technology, University of Groningen, Netherlands

[60] Nikhef, Science Park, Amsterdam, Netherlands

[61] ASTRON, Dwingeloo, Netherlands

[62] Institute of Nuclear Physics PAN, Krakow, Poland

[63] University of Łódź, Łódź, Poland

[64] Laboratório de Instrumentação e Física Experimental de Partículas - LIP and Instituto Superior Técnico - IST, Universidade de Lisboa - UL, Portugal

[65] 'Horia Hulubei' National Institute for Physics and Nuclear Engineering, Bucharest- Magurele, Romania

[66] Institute of Space Sciences, Bucharest, Romania

[67] University of Bucharest, Physics Department, Romania

[68] University Politehnica of Bucharest, Romania

[69] Experimental Particle Physics Department, J. Stefan Institute, Ljubljana, Slovenia

[70] Laboratory for Astroparticle Physics, University of Nova Gorica, Slovenia

[71] Universidad Complutense de Madrid, Madrid, Spain

[72] Universidad de Alcalá, Alcalá de Henares, Madrid, Spain

[73] Universidad de Granada and C.A.F.P.E., Granada, Spain

[74] Universidad de Santiago de Compostela, Spain

[75] School of Physics and Astronomy, University of Leeds, United Kingdom

[76] Case Western Reserve University, Cleveland, OH, USA

[77] Colorado School of Mines, Golden, CO, USA

[78] Colorado State University, Fort Collins, CO, USA

[79] Colorado State University, Pueblo, CO, USA

[80] Department of Physics and Astronomy, Lehman College, City University of New York, New York, USA

[81] Fermilab, Batavia, IL, USA

[82] Louisiana State University, Baton Rouge, LA, USA

[83] Michigan Technological University, Houghton, MI, USA

[84] New York University, New York, NY, USA

[85] Northeastern University, Boston, MA, USA

[86] Ohio State University, Columbus, OH, USA

[87] Pennsylvania State University, University Park, PA, USA

[88] University of Chicago, Enrico Fermi Institute, Chicago, IL, USA

[89] University of Hawaii, Honolulu, HI, USA

[90] University of Nebraska, Lincoln, NE, USA

[91] University of New Mexico, Albuquerque, NM, USA

(‡) Deceased

(a) Now at Konan University

(b) Also at the Universidad Autonoma de Chiapas on leave of absence from Cinvestav

(d) Now at Unidad Profesional Interdisciplinaria de Ingeniería y Tecnologías Avanzadas del IPN, México, D.F., México

(e) Now at Universidad Autónoma de Chiapas, Tuxtla Gutiérrez, Chiapas, México

(f) Also at Vrije Universiteit Brussels, Belgium

ABSTRACT

We present the results of an analysis of the large angular scale distribution

of the arrival directions of cosmic rays with energy above 4 EeV detected at the Pierre Auger Observatory including for the first time events with zenith angle between 60° and 80°. We perform two Rayleigh analyses, one in the right ascension and one in the azimuth angle distributions, that are sensitive to modulations in right ascension and declination, respectively. The largest departure from isotropy appears in the $E > 8$ EeV energy bin, with an amplitude for the first harmonic in right ascension $r_1^\alpha = (4.4 \pm 1.0) \times 10^{-2}$, that has a chance probability $P(\geq r_1^\alpha) = 6.4 \times 10^{-5}$, reinforcing the hint previously reported with vertical events alone.

Subject headings: astroparticle physics - cosmic rays

1. Introduction

The distribution of the arrival directions of cosmic rays, together with the spectrum and composition indicators, are the main observables to try to understand their origin and nature. The dipolar component of the large scale distribution of cosmic rays has been measured by different experiments at energies below 10^{17} eV (Amenomori et al. 2005, 2009; Guillian et al. 2007; Abdo et al. 2009; Aglietta et al. 2009; IceCube Collaboration 2011, 2012, 2013; Curcio et al. 2013), and has been searched for at higher energies by Hayashida et al. (1999) and the Pierre Auger Observatory. In the EeV ($\equiv 10^{18}$ eV) range the estimation of the large scale anisotropies can be useful to understand the transition from a Galactic to an extragalactic cosmic ray origin. The first hints of a change in the phase of the modulation in the right ascension distribution of arrival directions, happening around 1 EeV, are indeed suggested by the observations (The Pierre Auger Collaboration 2011a; Sidelnik 2013). At the highest energies, the presence of a significant dipole in the extragalactic cosmic ray distribution is a likely possibility. In particular, a dipolar flux could result from cosmic rays propagating diffusively in the extragalactic turbulent magnetic fields. This could happen if the amplitude of the field is large and/or if the cosmic rays have a component with large electric charge (Harari, Mollerach & Roulet 2014). A large angular scale anisotropy in the arrival direction distribution is also expected in the case that magnetic deflections are small if the cosmic ray sources are distributed similarly to the matter in the universe, due to the fact that in our local neighborhood matter is distributed inhomogeneously. These inhomogeneities lead in particular to the non-vanishing acceleration of the Local Group which is responsible for the peculiar velocity that gives rise to the observed dipole of the Cosmic Microwave Background (CMB) (Erdogdu et al. 2006). In fact, the non-isotropic distribution of the nearby extragalactic cosmic ray sources would lead to an excess of flux towards the direction with

the highest concentration of nearby sources and this would contribute to the dipolar component of the large scale distribution of arrival directions. The maximum redshift from which extragalactic cosmic rays can arrive at Earth progressively decreases as the energy threshold increases. This is a consequence of the energy losses due to pair production and photopion production by interactions with CMB photons in the case of protons, and to photodisintegration with the CMB and infrared (IR) backgrounds in the case of heavier nuclei (Greisen 1966; Zatsepin & Kuz'min 1966). Thus, the overall contribution of nearby sources becomes increasingly more important as the energy increases, leading to a larger expected anisotropy at higher energies.

The Pierre Auger Observatory has reported studies of the flux modulation in right ascension (The Pierre Auger Collaboration 2011a; Sidelnik 2013) and in both declination and right ascension (The Pierre Auger Collaboration 2012, 2013; de Almeida 2013) from the analysis of events with zenith angles smaller than 60°. Upper limits on the low ℓ multipolar amplitudes have also been reported from a joint analysis of the Pierre Auger Observatory and the Telescope Array data, taking advantage of the full sky coverage (The Pierre Auger and Telescope Array Collabo. 2014). In this paper we present an extension of the Pierre Auger Observatory studies including also for the first time inclined events with zenith angles between 60° and 80°. Given the location of the Pierre Auger Observatory at a latitude $-35.2°$, events arriving with zenith angles up to 60° cover sky directions with declinations $\delta \leq 24.8°$, corresponding to a fraction of 71% of the sky. By extending the zenith range up to 80°, declinations up to $\delta \leq 44.8°$ are observed, extending the accessible fraction of the sky to 85%.

2.   Pierre Auger Observatory and Data Set

The Pierre Auger Observatory (The Pierre Auger Collaboration 2004) consists of an array of 1660 water-Cherenkov detectors covering 3000 km^2 on a triangular grid of mostly 1.5 km spacing, the surface detector (SD). It also has 4 sites with 27 telescopes overlooking the array to observe the fluorescence light emitted by the showers (The Pierre Auger Collaboration 2010a), which allows a calorimetric measurement of the shower energy deposited in the atmosphere and is thus particularly useful for the calibration of the SD energy reconstruction. In contrast to the surface detector, the fluorescense detector (FD) has a smaller duty cycle of 13%.
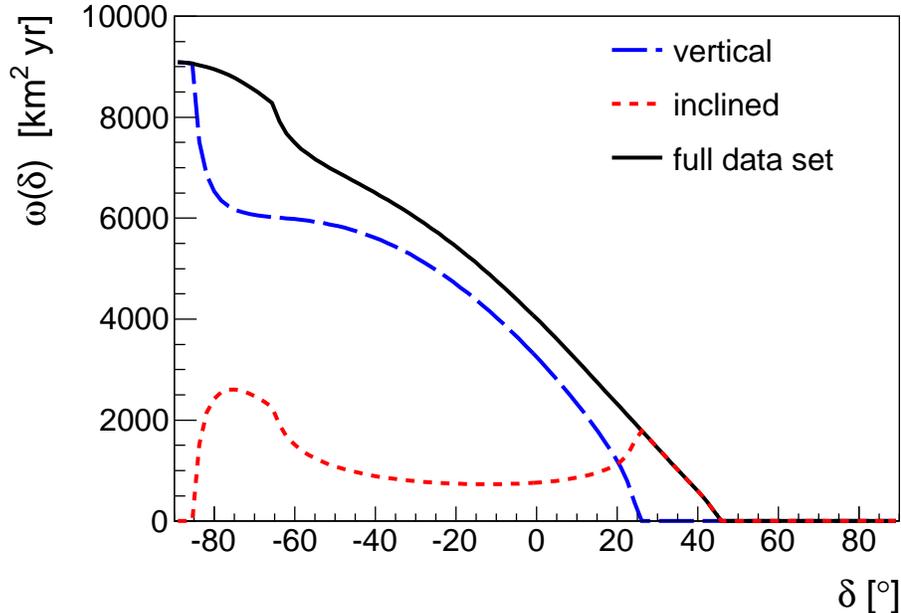
Fig. 1.— Directional exposure as a function of the declination, computed as in Sommers (2001). The long-dashed blue line corresponds to the vertical events, the short-dashed red one to the inclined events and the solid black line to the full data set.

2.1. Data Set

In this work, events recorded with the SD from 2004 January 1 to 2013 December 31 with zenith angle up to 80° are analyzed. The quality cut imposed on events with $\theta \leq 60°$ requires that all six neighbors of the water-Cherenkov detector with the largest signal be active at the time the event was recorded. In the case of events with $\theta > 60°$ the condition is defined differently and requires instead that the station nearest to the reconstructed core and its six neighbors be active. We also remove periods of instability on the data acquisition to have a reliable estimate of the detection exposure. The total geometric exposure, that applies to energies above full efficiency of the SD detector, is 48,029 km² sr yr in this period. The directional exposure as a function of the declination is shown in Figure 1 for events with zenith angle smaller than 60°, hereafter referred to as vertical events, for events with zenith from 60° to 80°, referred to as inclined events, and for all events. For vertical events full efficiency is attained at 3 EeV (The Pierre Auger Collaboration 2010b), while for inclined events, it is attained at 4 EeV. We will restrict the analysis to events with $E \geq 4$ EeV for which trigger effects are absent.

The event direction is determined from a fit to the arrival times of the shower front at

the surface detectors. The angular resolution depends on the number of stations involved in the event. For the energies considered in this study it is always better than 0.8°. The energy reconstruction procedure is different for events above and below 60°. For vertical events the shower size at 1000 m from the shower axis, $S(1000)$, is used. From $S(1000)$ the surface energy estimator S_{38}, corresponding to the signal that would have been measured had the shower arrived with a zenith angle of 38°, is obtained using the constant intensity cut method (The Pierre Auger Collaboration 2008). The S_{38} energy estimator is calibrated to the energy measured by the fluorescence detector for a subset of events detected by both the surface detector and the fluorescence one. The energy resolution is better than 17% (Pesce 2011). The constant intensity cut method exploits the fact that for full efficiency and an isotropic flux the arrival direction distribution $\mathrm{d}N/\mathrm{d}\sin^2\theta$ should be constant. As discussed in Appendix A of The Pierre Auger Collaboration (2012) a small deviation of this behavior, proportional to $(1 + d_z \sin\ell_{\mathrm{obs}}\cos\theta)$, is expected when a dipolar component along the Earth rotation axis d_z is present for an observation latitude ℓ_{obs}. This small modulation in the zenith angle distribution is not accounted for in this analysis. However, as it does not affect the distribution in azimuth, nor in right ascension, it does not affect the large scale analysis performed in this paper. Inclined showers require a specific energy reconstruction method because they are dominated by muons at ground. This method is based on the fact that the shape of the muon distribution is universal for a given shower direction and that only the overall normalization of the muon distribution depends on the shower energy. This allows us to define the energy estimator N_{19} as the overall normalization of a particular event with respect to a reference muon distribution, conventionally chosen to be the average muon density for primary protons of 10^{19} eV simulated with QGSJetII-03. Once the shower arrival direction is obtained, N_{19} is reconstructed by fitting the measured signals at the surface stations to the expected muon patterns (The Pierre Auger Collaboration 2014). Then, the energy of the cosmic rays is calibrated using a sub-sample of events reconstructed with both the fluorescence and surface array techniques, similarly to what is used to calibrate vertical events. The average energy resolution is 19.3%. The systematic uncertainty in the energy scale associated with the fluorescence detector energy assignment, applying to both vertical and inclined events, is 14% (Verzi 2013).

For $E \geq 4$ EeV the number of inclined events is 15,747, while that of vertical events is 54,467. The resulting ratio between the inclined and vertical integrated flux is 0.289 ± 0.003. Meanwhile, the expected ratio for a fully efficient detector and an isotropic flux is 0.293. The consistency of these ratios indicates that the energy calibrations of both data sets are compatible. This is expected as both energy estimators are calibrated with the energy measured by the fluorescence detector.

2.2. Atmospheric and Geomagnetic Field Effects

As the amplitudes of the large scale modulations to be measured are rather small, at the few percent level, it is very important to carefully account for spurious effects that can modulate the flux. Variations in the array effective size due to the deployment and dead times of the detectors are taken into account by introducing a weighting factor in the Rayleigh analysis, as discussed in the next section. Furthermore, due to the steepness of the energy spectrum, even small changes in the energy estimator as a function of time or the local angular coordinates would distort significantly the counting rate of events above a given energy. In particular, the atmospheric conditions affect the shower size $S(1000)$ due to two effects. As a larger (smaller) pressure corresponds to a larger (smaller) column density traversed, an air shower will be at a more (less) advanced stage of development when it arrives at the ground. Also the air density affects the Molière radius and hence the lateral profile of the showers. These atmospheric effects are here accounted for by correcting the energy estimator $S(1000)$ according to the weather conditions present at the time each event was recorded (The Pierre Auger Collaboration 2009).

The atmospheric conditions mainly affect the electromagnetic component of the showers, that is prominent in showers with zenith angles below 60°. For the more inclined showers the muonic component is dominant and the atmospheric effects are hence expected to be negligible. We have checked this assumption by measuring the flux modulation as a function of the solar time, where no intrinsic modulation of the flux is expected but where spurious modulations due to weather conditions are maximized. No significant solar modulation is indeed observed in inclined showers and thus no weather correction is applied to showers with zenith angles above 60°.

Another effect that influences the shower size at 1000 m is the deflection of the shower particles in the geomagnetic field. Such deflections break the circular symmetry of the shower around its axis and lead to an azimuthal modulation of $S(1000)$, as has been studied in detail for events with $\theta < 60°$ in The Pierre Auger Collaboration (2011b). If not taken into account in the energy estimator, this would induce an azimuthally dependent bias on the energy determination, leading to a spurious pseudo-dipolar pattern in the flux above a given energy threshold. In order to account for this effect and get an unbiased energy estimator, the measured shower size signal $S(1000)$ is related to the one that would have been observed in the absence of the geomagnetic field, and the latter is used to construct S_{38} (The Pierre Auger Collaboration 2011b). The reconstruction of events with $\theta > 60°$ takes into account the geomagnetic field effect already in the expected muon distributions used to reconstruct the energy estimator N_{19}, and thus no further correction is needed for the inclined events.

3. Modified Rayleigh Method

When combining two different data sets covering different regions of the sky, such as the vertical and inclined samples considered here, a small difference in the energy cross-calibration of the samples could give rise to a difference in the measured fluxes in those regions, that could translate in a spurious large scale modulation. We will hence adopt a method that is essentially insensitive to these effects, studying the large scale distribution of the arrival directions by performing a classical Rayleigh analysis (Linsley 1975) over both the right ascension and the azimuth angle distributions. The analysis is slightly generalized by weighting each event by a factor that takes into account small modulations in the exposure arising from the variations in the operating size of the array as a function of time, and for the effects of a small net tilt of the array surface (The Pierre Auger Collaboration 2012).

The number of active detector cells $n_{\rm cell}(t)$ (number of active detectors having their six neighbors active) is constantly monitored at the Observatory. The total number of active cells, $N_{\rm cell}$, as a function of the sidereal time α_0 (measured by the right ascension of the zenith at the center of the array) and its relative variations, $\Delta N_{\rm cell}$, are obtained from

$$N_{\rm cell}(\alpha_0) = \sum_j n_{\rm cell}(\alpha_0 + j\, T_{\rm sid}), \qquad \Delta N_{\rm cell}(\alpha_0) = \frac{N_{\rm cell}(\alpha_0)}{\langle N_{\rm cell}\rangle}, \tag{1}$$

with $\langle N_{\rm cell}\rangle = T_{\rm sid}^{-1}\int_0^{T_{\rm sid}} {\rm d}\alpha_0 N_{\rm cell}(\alpha_0)$, where $T_{\rm sid}$ corresponds to the duration of the sidereal day. The small modulations in right ascension of the flux induced by these variations is accounted for by weighting each event by a factor $w_i \propto \Delta N_{\rm cell}^{-1}(\alpha_0^i)$. The modulation in the total period of time considered has an amplitude of 0.24%, with the phase of the maximum at $\alpha_0 = 44°$. Note that the corresponding modulation at the solar frequency has instead a much larger amplitude of 3.5%, and it is the cancellation along the years, for 10 years of continuous operation of the Observatory, that leads to the small resulting amplitude at the sidereal frequency.

The geometric aperture of a horizontal array is given by $N_{\rm cell}(\alpha_0)\, a_{\rm cell}(\theta)$, where $a_{\rm cell}(\theta) = 1.95\cos\theta$ km^2 (The Pierre Auger Collaboration 2010b). However, the fact that the height above sea level of the array of detectors has a small average tilt of about $0.2°$ towards a direction $30°$ from the East to the South ($\phi_{\rm tilt} = -30°$) modulates the effective cell area according to

$$a_{\rm cell}(\theta,\phi) = 1.95[1 + 0.003\tan\theta\cos(\phi - \phi_{\rm tilt})]\cos\theta. \tag{2}$$

For energies above full efficiency the tilt effect can be taken into account by including in the weight of each event a factor $[1 + 0.003\tan\theta\cos(\phi - \phi_{\rm tilt})]^{-1}$ and neglecting the modulation in ϕ in the exposure.

The Fourier coefficients of the modified Rayleigh analysis in right ascension are then given by

$$a_k^\alpha = \frac{2}{\mathcal{N}} \sum_{i=1}^{N} w_i \cos(k\alpha_i), \qquad b_k^\alpha = \frac{2}{\mathcal{N}} \sum_{i=1}^{N} w_i \sin(k\alpha_i), \qquad (3)$$

where the sums run over the number of events N in the considered energy range, the weights are given by $w_i \equiv [\Delta N_{\text{cell}}(\alpha_0^i)(1 + 0.003\tan\theta_i \cos(\phi_i - \phi_{\text{tilt}}))]^{-1}$, and the normalization factor is $\mathcal{N} = \sum_{i=1}^{N} w_i$. The amplitude r_k^α and phase φ_k^α of the event rate modulation are estimated as

$$r_k^\alpha = \sqrt{(a_k^\alpha)^2 + (b_k^\alpha)^2}, \qquad \varphi_k^\alpha = \frac{1}{k}\arctan\frac{b_k^\alpha}{a_k^\alpha}. \qquad (4)$$

The weight factors w_i are very close to 1 in the present analysis, and thus the probability $P(\geq r_k^\alpha)$ that an amplitude equal to or larger than r_k^α arises from an isotropic distribution can be safely approximated by the cumulative distribution function of the Rayleigh distribution $P(\geq r_k^\alpha) = \exp(-\kappa_0)$, where $\kappa_0 = \mathcal{N}(r_k^\alpha)^2/4$.

The Fourier coefficients for the Rayleigh analysis in azimuth are given by the same expressions, just changing α by ϕ. Notice that after having accounted for the modulation induced by the tilt and the geomagnetic effect, the azimuthal distribution is expected to be uniform for energies above full efficiency for an isotropic distribution of cosmic rays. The amplitude b_1^ϕ is actually sensitive to asymmetries between the northern and southern local flux, and thus gives information on the dipolar component along the Earth's rotation axis.

We restrict the analysis to the first two harmonics $k = 1, 2$. The first harmonic coefficients in right ascension and azimuth are enough to reconstruct the dipole in the hypothesis that the higher order multipole contributions are negligible. The second harmonic coefficients ($k = 2$) give a measure of the quadrupole component of the cosmic ray distribution. We consider energies above the full efficiency of inclined events, splitting them in two bins, 4 to 8 EeV and $E > 8$ EeV, updating the results for the large scale anisotropy for the two highest energy bins reported in The Pierre Auger Collaboration (2011a, 2012); Sidelnik (2013); de Almeida (2013) with a larger sky coverage and nearly twice the number of events.

3.1. Right Ascension Distribution

The presence of an equatorial dipole component leads to non-vanishing coefficients a_1^α and/or b_1^α and hence to a non-vanishing amplitude r_1^α. In general, in an expansion in spherical harmonics ($\Phi(\delta, \alpha) = \sum_{\ell,m} a_{\ell m} Y^{\ell m}(\pi/2 - \delta, \alpha)$), all the terms $a_{\ell m}$ with $m = \pm k$ contribute to the a_k^α and b_k^α coefficients. In this section we present the results for the Rayleigh coefficients in right ascension and we will discuss the determination of the dipole in the next section. In

particular, a_1^α and b_1^α will be used to reconstruct the equatorial dipole in Section 4.1, while a_2^α and b_2^α probe the quadrupole.

The results for the modified Rayleigh analysis are quoted in Table 1 including the a_k^α and b_k^α coefficients with their statistical uncertainty $\sigma = \sqrt{2/\mathcal{N}}$, the amplitude r_k^α and phase φ_k^α, as well as the probability that a larger or equal amplitude arises by chance from an isotropic distribution.

Table 1: Rayleigh analysis in right ascension

E [EeV]	N	k	a_k^α	b_k^α	r_k^α	φ_k^α	$P(\geq r_k^\alpha)$
4 - 8	50,417	1	0.0030 ± 0.0063	0.0008 ± 0.0063	0.0031	15°	0.88
		2	-0.0012 ± 0.0063	-0.0004 ± 0.0063	0.0013	99°	0.98
> 8	19,797	1	-0.004 ± 0.010	0.044 ± 0.010	0.044	95°	6.4×10^{-5}
		2	0.009 ± 0.010	0.027 ± 0.010	0.028	36°	0.021

In the lower energy bin, between 4 and 8 EeV, all the coefficients are consistent with zero within their uncertainties, and there is no evidence for departures from isotropy in the right ascension distribution. In the higher energy bin, $E > 8$ EeV, the first harmonic has an amplitude $r_1^\alpha = 0.044 \pm 0.010$, with a chance probability to arise from an isotropic distribution of $P(\geq r_1^\alpha) = 6.4 \times 10^{-5}$. The phase φ_1^α points to 95°. Both the amplitude and the phase are in agreement with previous measurements reported in The Pierre Auger Collaboration (2011a); Sidelnik (2013). Due to the larger statistics, arising both from the larger time period considered as well as from the inclusion of the inclined events with $60° < \theta < 80°$, the significance of the measurement has grown to about 4σ. The amplitude of the second harmonic is less significant, with a 2% probability to arise by chance. We show in Figure 2 the ratio of the observed number of events to the mean number as a function of the right ascension, together with the first harmonic and the first plus second harmonics results.

A useful test to check if the systematic effects are well controlled is to repeat the analysis at the solar and the antisidereal frequencies. Each sidereal day is slightly shorter than the solar day by about 4 minutes. The antisidereal time is an artificial time scale in which the day is longer than a solar day by about 4 minutes, and therefore has 364.25 days per year. The weather and array size variations have the largest effect in producing spurious modulations at the solar frequency where the effects are not cancelled under the integration over several full years. No physical phenomena are expected to occur in the antisidereal frequency, however the combination of solar and seasonal systematic distortions could produce a spurious modulation in the antisidereal time. We report in Table 2 the results obtained
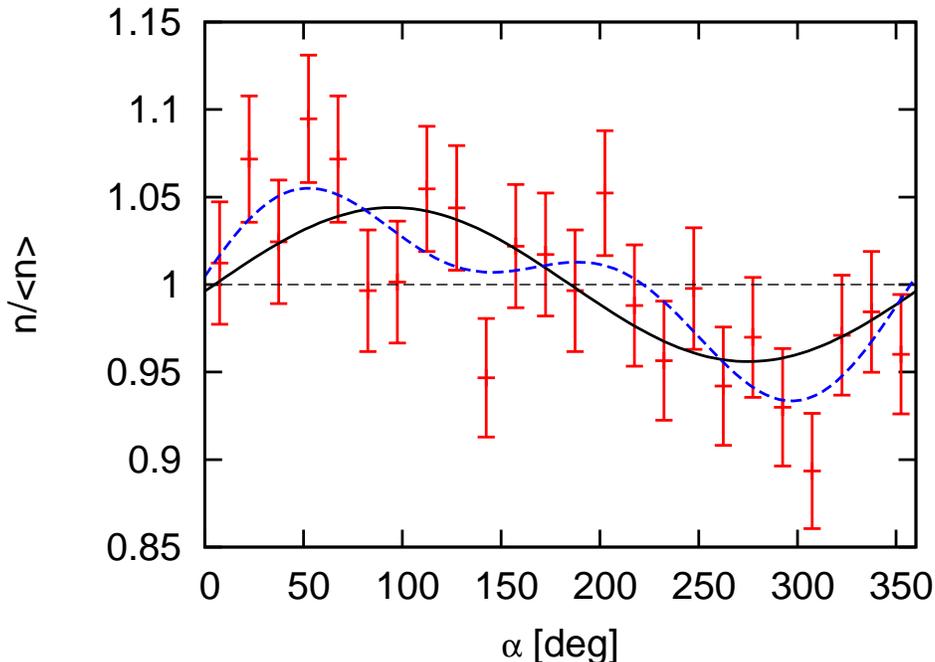
Fig. 2.— Observed number of events over the mean as a function of the right ascension with $1\,\sigma$ error bars for $E > 8$ EeV. The black solid line shows the first harmonic modulation from Table 1, while the blue dashed line shows the combination of the first and second harmonics.

after applying the weather correction and weighting the events with the factor to account for the modulation of the number of active detectors at the solar and antisidereal frequencies. No signs of spurious effects appear for any of the energy bins.

As a check that no large weather effect is present in the inclined events data set ($\theta > 60°$), we also performed the Rayleigh analysis at the solar frequency for all inclined events with $E \geq 4$ EeV. The amplitude obtained is $r_1^{\rm solar} = 0.012 \pm 0.011$, showing no sign of the presence of a weather modulation.

3.2. Azimuth Distribution

A dipolar component of the flux along the rotation axis of the Earth gives rise to a non-vanishing b_1^{ϕ} coefficient. Moreover, in general, each b_k^{ϕ} coefficient with odd k and each a_k^{ϕ} coefficient with even k receives contributions from all of the $a_{\ell 0}$ multipole coefficients with $\ell \geq k$ in a spherical harmonics expansion ($\Phi(\delta, \alpha) = \sum_{\ell,m} a_{\ell m} Y^{\ell m}(\pi/2 - \delta, \alpha)$). On the other hand, the a_k^{ϕ} coefficients with odd k and the b_k^{ϕ} with even k probe asymmetries

Table 2: First harmonic analysis in solar and antisidereal frequencies

	E [EeV]	r_1	φ_1 [h]	$P(\geq r_1)$
solar	4 - 8	0.0110 ± 0.0063	14	0.21
	> 8	0.005 ± 0.010	17	0.86
antisidereal	4 - 8	0.0046 ± 0.0063	8	0.76
	> 8	0.017 ± 0.010	13	0.24

between the eastern and western directions, that are expected to be zero when many full sidereal days are integrated. The results of the Rayleigh analysis in the azimuth angle are reported in Table 3.

Table 3: Rayleigh analysis in azimuth

E [EeV]	N	k	a_k^ϕ	b_k^ϕ	$P(\geq |a_k^\phi|)$	$P(\geq |b_k^\phi|)$
4 - 8	50,417	1	-0.0116 ± 0.0063	-0.0142 ± 0.0063	0.064	0.024
		2	-0.0034 ± 0.0063	-0.0066 ± 0.0063	0.59	0.29
> 8	19,797	1	-0.009 ± 0.010	-0.024 ± 0.010	0.35	0.015
		2	-0.006 ± 0.010	0.008 ± 0.010	0.58	0.45

The largest departure from isotropy appears for the b_1^ϕ coefficient in both energy bins, although with low statistical significance (2.4% and 1.5% probability, respectively). The a_2^ϕ coefficient that probes the quadrupolar component is subdominant (and compatible with zero) in both energy bins. The a_1^ϕ and b_2^ϕ coefficients are compatible with zero, as expected.

4.   Dipole Reconstruction

In this section the reconstruction of the dipole components from the Rayleigh coefficients obtained in the last section is performed, first in the simplified approximation that only the dipole contribution to large scale anisotropies is relevant, which is justified by the fact that the $k = 2$ coefficients determined in the previous section are not significantly different from zero. Then the reconstruction is performed considering also a possible quadrupole contribution. The reconstruction of the dipole (and quadrupole) components through this method does not require a precise knowledge of the directional acceptance of vertical and inclined events,

that would depend on the relative energy calibration of both samples. A miscalibration of one of the samples would just lead to a slight shift of the energy bins to which the events contribute, but without introducing a spurious modulation in right ascension or azimuth that could affect the determination of the dipole components.

4.1. Dipolar Pattern

A pure dipolar anisotropy can be parametrized as a function of the arrival direction $\hat{u}$ as

$$\Phi(\hat{u}) = \frac{\Phi_0}{4\pi}(1 + \vec{d} \cdot \hat{u}). \tag{5}$$

The observed arrival direction distribution is obtained by convoluting the flux with the detector exposure $\omega(\hat{u})$, giving

$$\frac{\mathrm{d}N}{\mathrm{d}\Omega}(\hat{u}) = \Phi(\hat{u})\,\omega(\hat{u}). \tag{6}$$

As a function of the local coordinates (θ,ϕ,α_0) the exposure ω can be considered to be a function of θ only, as the effects of the small modulation in ϕ and α_0 are already accounted for in the modified Rayleigh analysis. Assuming a general dipole with maximum amplitude d in the right ascension and declination direction (α_d,δ_d), and writing the angular dependence of the flux in terms of local coordinates[1], the first harmonic amplitudes in ϕ can be expressed by means of integrals of the flux as

$$a_1^\phi = \frac{2}{\mathcal{N}} \int_0^{2\pi} \mathrm{d}\alpha_0 \int_0^{2\pi} \mathrm{d}\phi \int_{\theta_{\min}}^{\theta_{\max}} \mathrm{d}\theta \sin\theta \cos\phi\, \Phi(\theta, \phi, \alpha_0) = 0, \tag{7}$$

$$b_1^\phi = \frac{2}{\mathcal{N}} \int_0^{2\pi} \mathrm{d}\alpha_0 \int_0^{2\pi} \mathrm{d}\phi \int_{\theta_{\min}}^{\theta_{\max}} \mathrm{d}\theta \sin\theta \sin\phi\, \Phi(\theta, \phi, \alpha_0) = \frac{\pi}{\mathcal{N}} \Phi_0 d_z \cos\ell_{\mathrm{obs}}\overline{\sin\theta}, \tag{8}$$

$$\mathcal{N} = \int_0^{2\pi} \mathrm{d}\alpha_0 \int_0^{2\pi} \mathrm{d}\phi \int_{\theta_{\min}}^{\theta_{\max}} \mathrm{d}\theta \sin\theta\, \Phi(\theta, \phi, \alpha_0) = \pi\Phi_0(\overline{1} + d_z \sin\ell_{\mathrm{obs}}\overline{\cos\theta}), \tag{9}$$

where in the last terms the integrals over ϕ and α_0 have been performed, d_z is the dipole component along the Earth's rotation axis, $d_z = d\sin\delta_d$, ℓ_{obs} is the latitude of the Observatory, and we denoted by $\overline{f(\theta)} \equiv \int_{\theta_{\min}}^{\theta_{\max}} \mathrm{d}\theta \sin\theta f(\theta)$. The coefficient a_1^ϕ vanishes as anticipated, while b_1^ϕ is related to d_z by

$$b_1^\phi = \frac{d_z \cos\ell_{\mathrm{obs}}\langle\sin\theta\rangle}{1 + d_z \sin\ell_{\mathrm{obs}}\langle\cos\theta\rangle}, \tag{10}$$

---

[1]Using the fact that $\hat{d} \cdot \hat{u} = \sin\delta_d(\cos\theta\sin\ell_{\mathrm{obs}} + \sin\theta\cos\ell_{\mathrm{obs}}\sin\phi) + \cos\delta_d\cos\alpha_d(-\sin\theta\cos\phi\sin\alpha_0 + \cos\theta\cos\ell_{\mathrm{obs}}\cos\alpha_0 - \sin\theta\sin\ell_{\mathrm{obs}}\sin\phi\cos\alpha_0) + \cos\delta_d\sin\alpha_d(\sin\theta\cos\phi\cos\alpha_0 + \cos\theta\cos\ell_{\mathrm{obs}}\sin\alpha_0 - \sin\theta\sin\ell_{\mathrm{obs}}\sin\phi\sin\alpha_0)$.

where we have used that $\overline{\sin\theta/1}$ can be estimated as the mean value of $\sin(\theta)$ of the events themselves, $\langle\sin\theta\rangle$, and similarly $\overline{\cos\theta/1} \simeq \langle\cos\theta\rangle$. Finally, for $d_z\sin\ell_{\rm obs}\langle\cos\theta\rangle \ll 1$, the dipole component along the Earth's rotation axis can be obtained to linear order as $d_z = b_1^\phi/(\cos\ell_{\rm obs}\langle\sin\theta\rangle)$.

On the other hand, the equatorial component of the dipole can be recovered from the Rayleigh analysis in right ascension, to linear order in the dipole amplitude, through $d_\perp \simeq r_1^\alpha/\langle\cos\delta\rangle$, where $\langle\cos\delta\rangle$ is the mean cosine declination of the events (The Pierre Auger Collaboration 2011a).

The resulting dipole components from the Rayleigh coefficients determined in the last section are reported in Table 4. The dipole component along the Earth's rotation axis d_z, the equatorial component $d_\perp$, the total amplitude d, as well as the direction $(\alpha_{\rm d}, \delta_{\rm d})$ are quoted for the two energy bins.

Table 4: Dipole components and directions in equatorial coordinates.

E [EeV]	d_z	$d_\perp$	d	$\delta_{\rm d}$	$\alpha_{\rm d}$
4 - 8	-0.027 ± 0.012	0.004 ± 0.008	0.027 ± 0.012	$-81° \pm 17°$	$15° \pm 115°$
> 8	-0.046 ± 0.019	0.057 ± 0.013	0.073 ± 0.015	$-39° \pm 13°$	$95° \pm 13°$

All of the dipole components obtained in both energy bins are compatible with the ones previously reported in The Pierre Auger Collaboration (2012); de Almeida (2013) within the systematic uncertainties.

4.2. Dipole and Quadrupole Patterns

Assuming now that the angular distribution of the flux can be well approximated by the combination of a dipole plus a quadrupole, it can be parametrized as

$$\Phi(\hat{u}) = \frac{\Phi_0}{4\pi}\left(1 + \vec{d}\cdot\hat{u} + \frac{1}{2}\sum_{i,j}Q_{ij}u_iu_j\right), \tag{11}$$

with Q_{ij} the symmetric and traceless quadrupole tensor. From the measured values of b_1^ϕ and a_2^ϕ obtained from the Rayleigh analysis in ϕ performed in the previous section, d_z and Q_{zz} can be determined through Eqs. (A3) and (A4), as discussed in the Appendix. From the right ascension Rayleigh coefficients a_2^α and b_2^α (and taking into account that Q_{ij} is traceless)

the quadrupole coefficients Q_{xy}, Q_{xx} and Q_{yy} can be determined through Eqs. (A10) and (A11) in the Appendix.

As a_1^α results from a combination of contributions from d_x and Q_{xz}, and b_1^α from a combination of d_y and Q_{yz}, two more independent measurements are needed to determine the four parameters. As discussed in the Appendix, a simple way of separating d_x and Q_{xz} is through computing a_1^α for the southern and northern subsamples of events, $a_1^{\alpha S}$ and $a_1^{\alpha N}$, obtained by restricting the sums in Eq. (3) to events with $\delta < 0$ and $\delta > 0$, respectively. Similarly, d_y and Q_{yz} can be separated by measuring $b_1^{\alpha S}$ and $b_1^{\alpha N}$.

In Table 5 we report the first harmonics in right ascension for the events coming from the southern and northern hemispheres for the two energy bins considered.

Table 5: First harmonic in right ascension for events arriving from the southern and northern hemispheres.

E [EeV]	Hem	N	a_1^α	b_1^α	r_1^α	φ_1^α	$P(\geq r_1^\alpha)$
4 - 8	S	40,256	0.0034 ± 0.0070	-0.0010 ± 0.0070	0.0036	344°	0.88
	N	10,161	0.001 ± 0.014	0.008 ± 0.014	0.008	79°	0.85
> 8	S	15,878	-0.005 ± 0.011	0.042 ± 0.011	0.042	96°	7.9×10^{-4}
	N	3919	-0.001 ± 0.022	0.051 ± 0.022	0.051	91°	0.075

In the energy bin between 4 and 8 EeV the amplitude in both hemispheres is compatible with zero within the uncertainties. This means that the fact that the r_1^α amplitude for the full data set vanishes as reported in Table 1 is not due to a cancellation of two significant and opposite modulations in the northern and the southern hemispheres. For $E > 8$ EeV the modulation is more significant and has the same phase in both hemispheres, indicating that the dipolar contribution to the modulation dominates over the quadrupolar one.

Table 6 reports the dipolar and quadrupolar reconstructed components. In both energy bins the reconstructed dipolar components are consistent with those reported in Table 4 in the hypothesis of a pure dipolar anisotropy. The most significant quadrupole component is the Q_{xy} one in the $E > 8$ EeV bin, that according to Eq. (A10) is proportional to the second harmonic in right ascension b_2^α, whose amplitude has a 2% probability to arise by chance from isotropy (see Table 1).

We show in Fig. 3 the sky maps in equatorial coordinates of the flux of cosmic rays, in units of km^{-2} yr^{-1} sr^{-1}, smoothed in an angular window of 45° for the two energy bins considered. The upper panel corresponds to the energy bin between 4 and 8 EeV, while

Table 6: Reconstruction with dipole and quadrupole patterns

E [EeV]	d_i	Q_{ij}
4 - 8	$d_z = -0.012 \pm 0.030$	$Q_{zz} = 0.028 \pm 0.052$
	$d_x = 0.003 \pm 0.010$	$Q_{xx} = -0.018 \pm 0.032$
	$d_y = 0.005 \pm 0.010$	$Q_{xy} = -0.001 \pm 0.019$
		$Q_{xz} = -0.004 \pm 0.024$
		$Q_{yz} = 0.013 \pm 0.024$
> 8	$d_z = -0.021 \pm 0.048$	$Q_{zz} = 0.046 \pm 0.083$
	$d_x = -0.003 \pm 0.016$	$Q_{xx} = 0.004 \pm 0.051$
	$d_y = 0.055 \pm 0.016$	$Q_{xy} = 0.080 \pm 0.030$
		$Q_{xz} = 0.007 \pm 0.039$
		$Q_{yz} = -0.004 \pm 0.039$

the lower panel corresponds to $E > 8$ EeV. Notice the difference in the color scales of flux variations appearing in the two plots. While for the high energy bin the maximum flux is 21% larger than the minimum one, for the lower energy bin this ratio is just 8%.

5.   Conclusions

We presented the results of an analysis of the large angular scale distribution of the arrival directions of the Pierre Auger Observatory data including for the first time inclined events with zenith angle between 60° and 80°. The inclusion of the inclined events not only provides an increase of about 30% in the number of events, but also leads to a larger fraction of the sky covered, up to 85%. We performed two Rayleigh analyses, in the right ascension and azimuth angles, that are sensitive to the right ascension and declination modulation of the flux, respectively. Two energy bins above the full efficiency for inclined events were analyzed: from 4 to 8 EeV and above 8 EeV. No significant departure from isotropy is observed in the distribution of events in the energy bin between 4 and 8 EeV. For energies above 8 EeV the first harmonic in right ascension has an amplitude $r_1^\alpha = (4.4 \pm 1.0) \times 10^{-2}$ with a chance probability $P(\geq r_1^\alpha) = 6.4 \times 10^{-5}$, reinforcing the hint reported in Sidelnik (2013) with vertical events alone detected up to the end of 2012.

The Rayleigh analysis in azimuth, sensitive to modulations in the declination direction, gives first harmonic coefficients $b_1^\phi = -0.014 \pm 0.006$ for energies between 4 and 8 EeV and $b_1^\phi = -0.024 \pm 0.010$ for energies larger than 8 EeV. The negative values in both energy bins

correspond to a dipolar component d_z pointing to the South, although the amplitudes have low statistical significance, with chance probabilities of 2.4% and 1.5%, respectively.

Under the assumption that the only significant contribution to the anisotropy is from the dipolar component, the observations above 8 EeV correspond to a dipole of amplitude $d = 0.073 \pm 0.015$ pointing to $(\alpha, \delta) = (95° \pm 13°, -39° \pm 13°)$. If a quadrupolar contribution is also included, the resulting dipole is consistent with that obtained in the previous case, although with a larger uncertainty, and the quadrupole components obtained are not significant.

A.   APPENDIX: RECONSTRUCTION OF DIPOLAR AND QUADRUPOLAR COMPONENTS

We present here the reconstruction of the dipolar and quadrupolar components in the case where the angular distribution of the flux at Earth can be well approximated by the combination of a dipole plus a quadrupole. In this case the flux can be parametrized as in eq. (11).

Analogously to eq. (8) in this case b_1^ϕ and a_2^ϕ can be written by direct integration in terms of d_z and Q_{zz} as

$$b_1^\phi = \frac{\pi}{\mathcal{N}}\Phi_0 \cos \ell_{\rm obs} \left(d_z \overline{\sin \theta} + \frac{3}{2}Q_{zz} \sin \ell_{\rm obs} \overline{\sin \theta \cos \theta} \right), \tag{A1}$$

$$a_2^\phi = -\frac{3\pi}{8\mathcal{N}}\Phi_0 \cos^2 \ell_{\rm obs} \overline{\sin^2 \theta} Q_{zz}. \tag{A2}$$

Then, from the measured values of b_1^ϕ and a_2^ϕ, and using that to leading order $\mathcal{N} \simeq \pi\Phi_0\overline{1}$, d_z and Q_{zz} can be determined as

$$d_z = \frac{1}{\langle \sin \theta \rangle \cos \ell_{\rm obs}} \left(b_1^\phi + 4a_2^\phi \tan \ell_{\rm obs} \frac{\langle \sin \theta \cos \theta \rangle}{\langle \sin^2 \theta \rangle} \right), \tag{A3}$$

$$Q_{zz} = -\frac{8}{3}\frac{a_2^\phi}{\cos^2 \ell_{\rm obs} \langle \sin^2 \theta \rangle}. \tag{A4}$$

The right ascension Rayleigh coefficients are also obtained from direct integration as

$$a_k^\alpha = \frac{2}{\mathcal{N}} \int_{\delta_{\min}}^{\delta_{\max}} d\delta \cos\delta \, \omega(\delta) \int_0^{2\pi} d\alpha \cos(k\alpha) \, \Phi(\delta, \alpha), \tag{A5}$$

where $\delta_{\min}$ and $\delta_{\max}$ are the minimum and maximum declination considered ($-90°$ and $44.8°$ respectively, when the full data set is considered). The coefficient b_k^α is given by a similar expression changing $\cos(k\alpha)$ to $\sin(k\alpha)$. Then,

$$a_1^\alpha = \frac{\Phi_0}{2\mathcal{N}} \left(d_x \widetilde{\cos\delta} + Q_{xz} \widetilde{\cos\delta \sin\delta} \right), \tag{A6}$$

$$b_1^\alpha = \frac{\Phi_0}{2\mathcal{N}} \left(d_y \widetilde{\cos\delta} + Q_{yz} \widetilde{\cos\delta \sin\delta} \right), \tag{A7}$$

$$a_2^\alpha = \frac{\Phi_0}{8\mathcal{N}} (Q_{xx} - Q_{yy}) \widetilde{\cos^2\delta}, \tag{A8}$$

$$b_2^\alpha = \frac{\Phi_0}{4\mathcal{N}} Q_{xy} \widetilde{\cos^2\delta}, \tag{A9}$$

where we denoted $\widetilde{f(\delta)} \equiv \int_{\delta_{\min}}^{\delta_{\max}} d\delta \cos\delta \, \omega(\delta) f(\delta)$, and to leading order $\mathcal{N} \simeq \Phi_0 \widetilde{1}/2$. From the last two equations, we obtain that

$$Q_{xy} = \frac{2b_2^\alpha}{\langle \cos^2\delta \rangle}, \tag{A10}$$

$$Q_{xx} - Q_{yy} = \frac{4a_2^\alpha}{\langle \cos^2\delta \rangle}, \tag{A11}$$

where we have used that $\widetilde{\cos^2\delta}/\widetilde{1}$ can be estimated by the mean value $\langle \cos^2\delta \rangle$ of the events. Taking into account that the quadrupole tensor is traceless, from Eqs. (A4) and (A11) the three diagonal terms can be obtained.

The d_x and Q_{xz} components appear combined in a_1^α (and similarly d_y and Q_{yz} in b_1^α), and cannot be disentangled by just measuring the first harmonic amplitudes in right ascension for the full data set, as both coefficients represent a modulation proportional to $\cos\alpha$. The difference is that the modulation induced by d_x is symmetric with respect to the equatorial plane (same sign in the northern and southern hemispheres) while that induced by Q_{xz} is antisymmetric (opposite sign in the northern and southern hemispheres). Then a simple way of separating d_x and Q_{xz} is computing a_1^α for the southern and northern subsamples of events, $a_1^{\alpha S}$ and $a_1^{\alpha N}$, restricting the sums in Eq. (3) to events with $\delta < 0$ and $\delta > 0$, respectively. Similarly d_y and Q_{yz} can be separated by measuring $b_1^{\alpha S}$ and $b_1^{\alpha N}$. From Eqs. (A6) and (A7) we can write

$$a_1^{\alpha S(N)} = d_x \langle \cos\delta \rangle_{S(N)} + Q_{xz} \langle \cos\delta \sin\delta \rangle_{S(N)}, \tag{A12}$$

$$b_1^{\alpha S(N)} = d_y \langle \cos\delta \rangle_{S(N)} + Q_{yz} \langle \cos\delta \sin\delta \rangle_{S(N)}, \tag{A13}$$

where $\langle\cdot\rangle_{\mathrm{S}}$ and $\langle\cdot\rangle_{\mathrm{N}}$ denote the mean values over the events from the southern and northern hemispheres, respectively. We can then estimate the corresponding dipolar and quadrupolar components as

$$d_x = \frac{a_1^{\alpha\mathrm{S}}\langle\cos\delta\sin\delta\rangle_{\mathrm{N}} - a_1^{\alpha\mathrm{N}}\langle\cos\delta\sin\delta\rangle_{\mathrm{S}}}{\langle\cos\delta\rangle_{\mathrm{S}}\langle\cos\delta\sin\delta\rangle_{\mathrm{N}} - \langle\cos\delta\rangle_{\mathrm{N}}\langle\cos\delta\sin\delta\rangle_{\mathrm{S}}}, \tag{A14}$$

$$Q_{xz} = \frac{a_1^{\alpha\mathrm{S}}\langle\cos\delta\rangle_{\mathrm{N}} - a_1^{\alpha\mathrm{N}}\langle\cos\delta\rangle_{\mathrm{S}}}{\langle\cos\delta\rangle_{\mathrm{N}}\langle\cos\delta\sin\delta\rangle_{\mathrm{S}} - \langle\cos\delta\rangle_{\mathrm{S}}\langle\cos\delta\sin\delta\rangle_{\mathrm{N}}}, \tag{A15}$$

and

$$d_y = \frac{b_1^{\alpha\mathrm{S}}\langle\cos\delta\sin\delta\rangle_{\mathrm{N}} - b_1^{\alpha\mathrm{N}}\langle\cos\delta\sin\delta\rangle_{\mathrm{S}}}{\langle\cos\delta\rangle_{\mathrm{S}}\langle\cos\delta\sin\delta\rangle_{\mathrm{N}} - \langle\cos\delta\rangle_{\mathrm{N}}\langle\cos\delta\sin\delta\rangle_{\mathrm{S}}}, \tag{A16}$$

$$Q_{yz} = \frac{b_1^{\alpha\mathrm{S}}\langle\cos\delta\rangle_{\mathrm{N}} - b_1^{\alpha\mathrm{N}}\langle\cos\delta\rangle_{\mathrm{S}}}{\langle\cos\delta\rangle_{\mathrm{N}}\langle\cos\delta\sin\delta\rangle_{\mathrm{S}} - \langle\cos\delta\rangle_{\mathrm{S}}\langle\cos\delta\sin\delta\rangle_{\mathrm{N}}}. \tag{A17}$$

REFERENCES

Aab, A.,Abreu, P., Aglietta, M., et al. (The Pierre Auger Collaboration) 2014, JCAP, 08, 019.

Aab, A.,Abreu, P., Aglietta, M., et al. (The Pierre Auger and Telescope Array Collaborations) 2014, ApJ, 794, 172

Aartsen, M. G., Abbasi, R., Abdou, Y., et al. (IceCube Collaboration) 2013, ApJ, 765, 55

Abbasi, R., Abdou, Y., Abu-Zayyad, T., et al. (IceCube Collaboration) 2011, ApJ., 740, 16

Abbasi, R., Abdou, Y., Abu-Zayyad, T., et al. (IceCube Collaboration) 2012, ApJ., 746, 33

Abdo, A. A., Allen, B. T., Aune, T., et al. 2009, ApJ, 698, 2121

Abraham, J., Aglietta, M., Aguirre, I. C., et al. (The Pierre Auger Collaboration) 2004, NIMPA, 523, 50

Abraham, J., Abreu, P., Aglietta, M., et al. (The Pierre Auger Collaboration) 2008, PhRvL, 101, 061101

Abraham, J., Abreu, P., Aglietta, M., et al. (The Pierre Auger Collaboration) 2009, APh, 32, 89

Abraham, J., Abreu, P., Aglietta, M., et al. (The Pierre Auger Collaboration) 2010a, NIMPA, 620, 227

Abraham, J., Abreu, P., Aglietta, M., et al. (The Pierre Auger Collaboration) 2010b, NIMPA, 613, 29

Abreu, P., Aglietta, M., Ahn, E. J. et al. (The Pierre Auger Collaboration) 2011a, APh, 34, 627

Abreu, P., Aglietta, M., Ahn, E. J. et al. (The Pierre Auger Collaboration) 2011b, JCAP, 11, 022

Abreu, P., Aglietta, M., Ahlers M. et al. (The Pierre Auger Collaboration) 2012, ApJS, 203, 34

Abreu, P., Aglietta, M., Ahlers M. et al. (The Pierre Auger Collaboration) 2013, ApJL, 762, L13

Aglietta, M., Alekseenko, V. V., Alessandro, B., et al. (The EAS-TOP Collaboration) 2009, ApJ, 692, L130

Amenomori, M., Ayabe S., Cui S. W., et al. (The Tibet AS Gamma Collaboration) 2005, ApJL, 626, L29

Amenomori, M., Bi, X. J., Chen, D., et al. 2009, 31st International Cosmic Ray Conference, Lodz, Poland

Curcio, C., Apel, W. D., Arteaga-Velazquez, J. C., et al. (KASCADE-Grande Collaboration) 2013, Proc. 33rd International Cosmic Ray Conference, Rio de Janeiro, Brazil

de Almeida, R. (for The Pierre Auger Collaboration) 2013, 33rd International Cosmic Ray Conference, Rio de Janeiro, Brazil (arXiv:1307.5059)

Erdogdu P., Lahav, O., Huchra, J. P., et al. 2006, MNRAS 368, 1515

Greisen, K. 1966, PhRvL, 16, 748

Guillian, G., Hosaka, J., Ishihara K., et al.(The Super-Kamiokande Collaboration) 2007, PhRvD, 75, 062003

Harari, D., Mollerach, S. & Roulet, E. 2014, PhRvD, 89, 123001

Hayashida, N., Honda, K., Inoue, N., et al. 1999, APh, 10, 303

Linsley, J. 1975, PhRvL, 34, 1530

Pesce, R. (for The Pierre Auger Collaboration) 2011, Proc. 32nd International Cosmic Ray Conference, Beijing, China (arXiv:1107.4809)

Sidelnik, I. (for The Pierre Auger Collaboration) 2013, Proc. 33$^{\rm rd}$ International Cosmic Ray Conference, Rio de Janeiro, Brazil (arXiv:1307.5059)

Sommers, P. 2001, APh, 14, 71

Verzi, V. (for The Pierre Auger Collaboration) 2013, Proc. 33$^{\rm rd}$ International Cosmic Ray Conference, Rio de Janeiro, Brazil (arXiv:1307.5059)

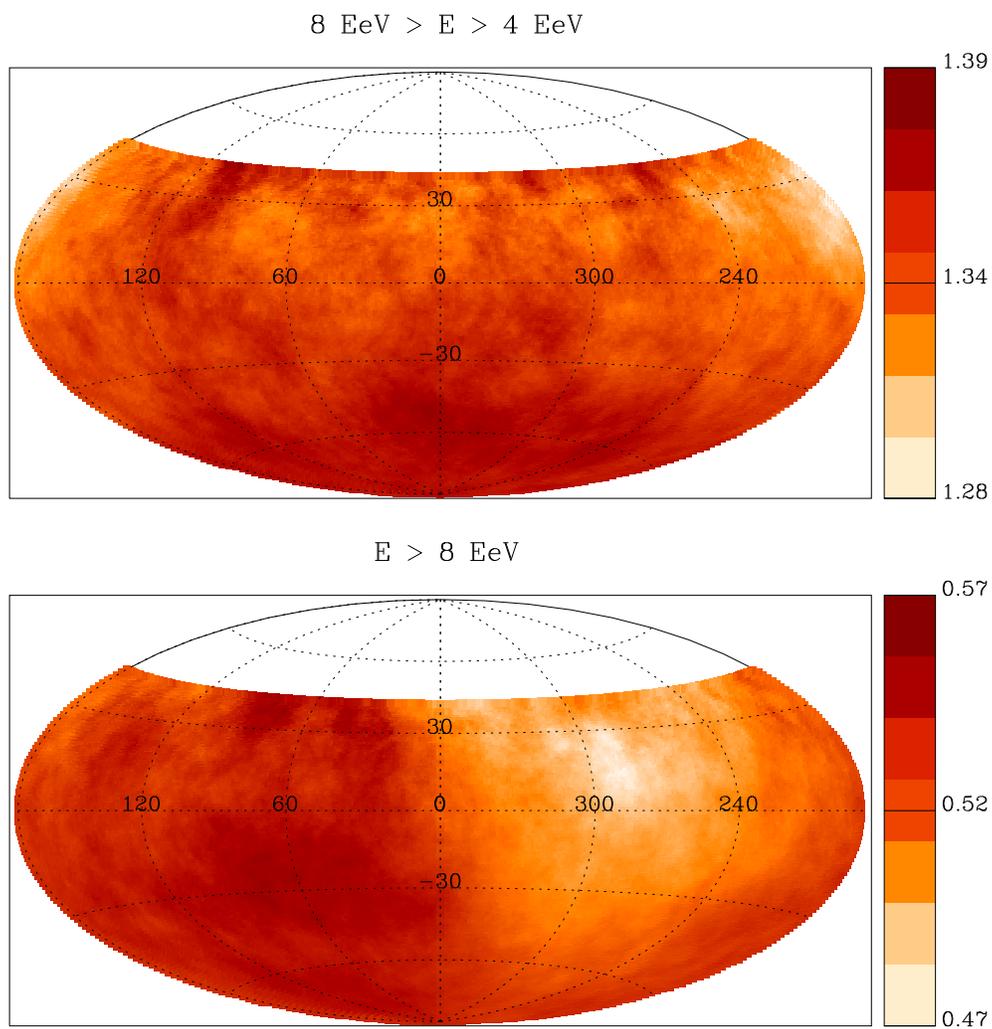Zatsepin G. T. and Kuz'min V. A. 1966, Sov. Phys. JETP Lett., 4, 78

Fig. 3.— Sky map in equatorial coordinates of flux, in km^{-2} yr^{-1} sr^{-1} units, smoothed in angular windows of 45° and for the two energy bins.